


EXPRESS LETTER

Open Access



Paleomagnetism and paleomagnetic dating to large volcanic bombs: an example from the historical eruption of Azuma–Jododaira volcano, NE Japan

Takeshi Hasegawa^{1*} , Bunta Kikuchi², Shohei Shibata¹, Yuhji Yamamoto³, Takumi Imura⁴, Masao Ban⁴, Kae Tsunematsu⁴, Chie Kusu¹, Makoto Okada¹ and Tsukasa Ohba⁵

Abstract

Vulcanian activity is one of the most common eruption styles of arc andesitic volcanism on Earth. It ejects and deposits volcanic bombs around the source crater. Although paleomagnetic studies of volcanic bombs are limited, such studies can potentially provide more opportunities for high-resolution paleomagnetic dating of volcanic activity. In this study, paleomagnetic dating was applied to large (> 1 m) volcanic bombs around active craters in the Azuma volcano group, NE Japan. Oriented samples were collected from the interior parts of five large volcanic bombs situated on gentle slopes, a few hundred meters from the source crater. More than six core samples were collected from each bomb and all samples were subjected to a range of rock magnetic experiments, including anisotropy of magnetic susceptibility (AMS) and thermal/alternating field demagnetization (THD/AFD) analyses. The Characteristic Remanent Magnetization (ChRM) directions for specimens from all bombs were well-defined, have small α_{95} (< 2.5°), and are in close agreement with each other. Comparing our measured overall mean direction ($D_m = 355.5^\circ$, $I_m = 49.8^\circ$, $\alpha_{95} = 1.6^\circ$) with modeled geomagnetic field estimates and a reference secular variation curve for this area (using MATLAB-based archaeomagnetic dating tool), we suggest that the volcanic bombs were produced in the historical Meiji period (1893–1895 CE) eruption. In addition, a combination of the data of ChRM, AMS, thermomagnetic analyses, hysteresis measurement, and XRF analysis indicates that the volcanic bombs were derived from a plug of lava in the conduit under the solidification point (ca. 800 °C), but above the Curie point of the titanomagnetite remanence carrier (around 300 °C). We show that volcanic bombs can be powerful for paleomagnetic dating if certain sampling conditions, such as quantity, situation, size and portion are satisfied.

Keywords Paleomagnetic dating, Volcanic bomb, Rock magnetism, Azuma volcano group, Vulcanian eruptions

*Correspondence:

Takeshi Hasegawa

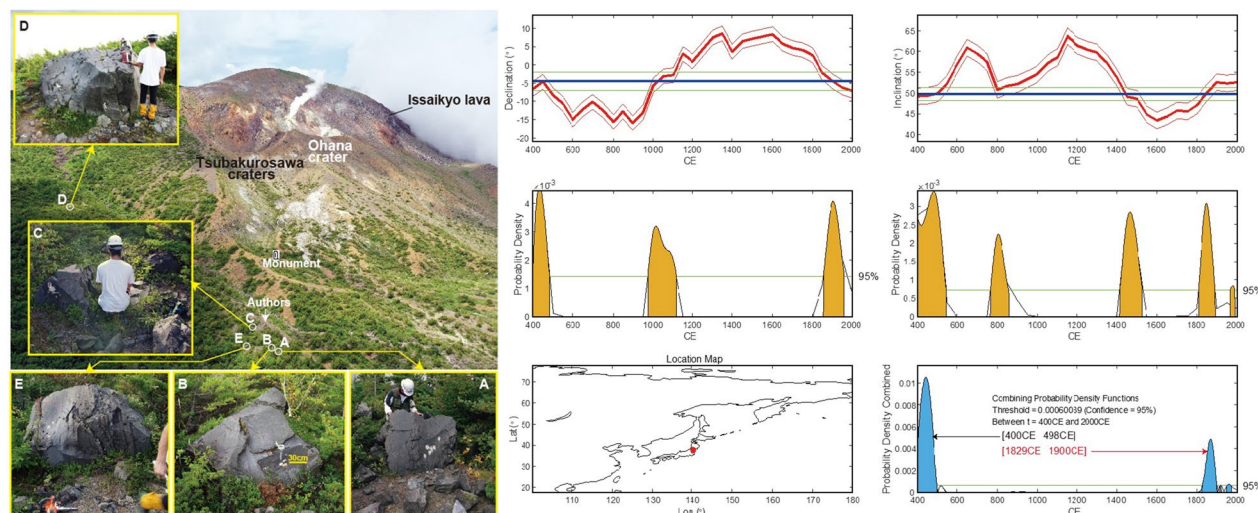
takeshi.hasegawa.paul@vc.ibaraki.ac.jp

Full list of author information is available at the end of the article



© The Author(s) 2023, corrected publication 2023. **Open Access** This article is licensed under a Creative Commons Attribution 4.0 International License, which permits use, sharing, adaptation, distribution and reproduction in any medium or format, as long as you give appropriate credit to the original author(s) and the source, provide a link to the Creative Commons licence, and indicate if changes were made. The images or other third party material in this article are included in the article's Creative Commons licence, unless indicated otherwise in a credit line to the material. If material is not included in the article's Creative Commons licence and your intended use is not permitted by statutory regulation or exceeds the permitted use, you will need to obtain permission directly from the copyright holder. To view a copy of this licence, visit <http://creativecommons.org/licenses/by/4.0/>.

Graphical Abstract



Introduction

In recent decades, paleomagnetic dating has been increasingly applied to volcanic rocks, such as lava and welded tuff. Eruption ages can be estimated by comparing measured paleomagnetic directions and intensities of volcanic rocks with paleosecular variation (PSV) curves (e.g., Böhnell et al. 2016; Greve and Turner 2017). Furthermore, the resolution of PSV curves, recording the past few thousand years, has highly improved in recent studies (e.g., Tanguy et al. 2003; Arrighi et al. 2006; Speranza et al. 2008; Hatakeyama 2013; Roperch et al. 2015; Turner and Corkill 2023). Considering geomagnetic direction changes of 0.05–0.20°/year, eruption ages with a time resolution of a few tens of years can be obtained when the mean ChRM direction of a volcanic rock is determined with a small α_{95} ($< 3.0^\circ$). In a recent study (Hasegawa et al. 2023), we acquired precise ($\alpha_{95} < 3.0^\circ$) paleomagnetic directions from unconsolidated (non-welded) tephras, including air fall deposits. The applicability of paleomagnetic dating for volcanic rocks is expanding to ash layers with this technique (Hasegawa et al. 2023). Paleomagnetic dating can yield not only the eruption age but also the duration of a single eruptive event and intervals (time gaps) of successive eruptions (e.g., Pivarunas et al. 2022; Hasegawa et al. 2023; Kósik et al. 2023).

On the other hand, the traditional ^{14}C dating method has also usually been applied to determine the age of young (< 60 ka) eruption episodes. The resolution of ^{14}C dating can be higher (less than tens of years) than that of paleomagnetic methods (e.g., ^{14}C wiggle-match method: Kojo et al. 1994). However, the ^{14}C method requires

suitable organic materials, such as charcoal and paleosol, that are rarely found within lavas and volcanic bombs. One of the advantages of the paleomagnetic method is that we can use eruption products directly. To establish a tight age constraint of volcanic activity consisting of various eruption styles, combining the paleomagnetic and ^{14}C methods would be effective.

Vulcanian eruptions are one of the most common eruption styles on Earth, especially from andesitic volcanoes that eject and deposit volcanic bombs around the source crater. Only a few paleomagnetic studies focusing on volcanic bombs have been published (e.g., Cañón-Tapia 2017; Cole et al. 2019), and these studies were aimed at investigating formation mechanisms and emplacement conditions, such as temperature. Difficulties of using volcanic bombs for paleomagnetic dating include the possibility of in-flight cooling and secondary movement after the acquisition of thermal demagnetization. However, if we can obtain appropriate paleomagnetic data from volcanic bombs, it can provide more valuable opportunities to date the volcanic activity that produced the bombs.

Here, we show how careful sampling and analysis of large volcanic bombs can provide reliable paleomagnetic ages. The samples were obtained from historical eruption products from the Azuma volcano group, which is one of the most active volcanoes in NE Japan. As a result of careful sampling and paleomagnetic analyses, the volcanic bomb samples yielded useful data that enabled us to re-define the historical eruption age. Although the main dating results have been reported elsewhere (Hasegawa et al. 2023), in the current study we

have added the results of alternating field demagnetization (AFD), anisotropy of magnetic susceptibility (AMS), thermomagnetic analyses, hysteresis measurement, and XRF analysis to investigate the carrier magnetic minerals, and the magnetization acquisition processes of the volcanic bombs. Moreover, the MATLAB-based archaeomagnetic dating tool of Pavón-Carrasco et al. (2011) allowed us to obtain quantitative estimates of the age and its probability distribution. These new results are presented in this paper.

Azuma–Jododaira volcano

The Azuma volcano group consists of E–W-trending composite cones located in the central part of the volcanic front of NE Japan. The eastern part of the volcano group is composed of several volcanic peaks, such as Mt. Issaikyozan (elevation 1,949 m), Maedaiten and Higashiazumayama (Fig. 1). An amphitheater-like large (>2 km in diameter) depression surrounded by these volcanic peaks, named Jododaira, forms and opens to the east. In Jododaira, pyroclastic cones, such as Azumakofuji and Okenuma, as well as multiple craters (Fig. 1) were generated during the Holocene (Yamamoto 2005). The Holocene volcanic area within Jododaira is generally referred to as “Azuma–Jododaira volcano” and is defined as an active volcano in Japan (Yamamoto 2005; Matsumoto, et al. 2018). The Ohana and Tsubakurosawa craters are located on the southeastern flank of Mt. Issaikyozan

(Fig. 1) and are the most active with notable continuous fumarolic activity today (Fig. 2).

Mount Issaikyozan lava (Issaikyo lava) shows a wide range of K–Ar ages from 500 to 180 ka (Matsumoto, et al. 2018). The age and formation process of Jododaira has not been clearly defined (Furukawa et al. 2018). Azumakofuji, the most prominent cone of Azuma–Jododaira volcano is composed of lava flows, strombolian ejecta, and vulcanian tephra that give ^{14}C and tephrochronologic ages of 6–5 ka (Yamamoto 2005). Subsequent activity related to multiple craters, including Iwodaira–Minami, Ohana, and Tubakurosawa craters, have been geologically studied by Yamamoto (2005) and Imura et al. (2021). However, the detailed stratigraphy and ages are still unclear.

Based on the summary of historical accounts by Yamamoto (2005), the oldest eruption occurred in the Kamakura period (1333 CE) from Ohana crater. The next was the Edo period eruption around 1711 CE (Yamamoto 2005), followed by the Meiji period eruption of 1893–1895 CE that occurred at the Tsubakurosawa craters (Fig. 1). There is no geophysical observation record, but many detailed field surveys and eyewitness accounts of the Meiji period eruption exist (e.g., Omori 1893; Yokoyama 1893). Two investigators, Mr. Miura and Mr. Nishiyama from the Japan Geological Survey were killed during their field survey of the 7th June, 1893 eruption. After the Meiji period eruption, phreatic eruptions were recorded and

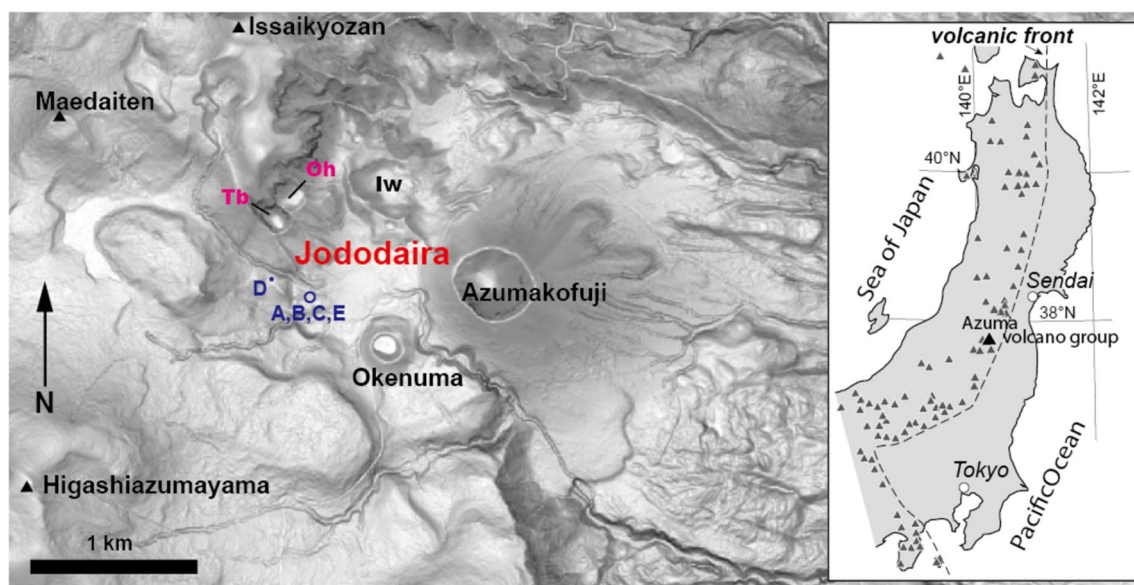


Fig. 1 Index map of Azuma–Jododaira volcano after Hasegawa et al. (2023). The base slope gradation map is provided by the Geospatial Information Authority of Japan (GSI) as a part of the GSI Tiles collection. A dot and circle with blue labels (A–E) are the locations of oriented sampling for large breadcrust bombs (see Fig. 2). *Tb* Tsubakurosawa craters, *Oh* Ohana crater, *Iw* Iwodaira–Minami crater. Triangles: peaks of strato-cones consisting of eastern Azuma volcano group. Inset shows the volcanic front of NE Japan and the situation of Azuma volcano group

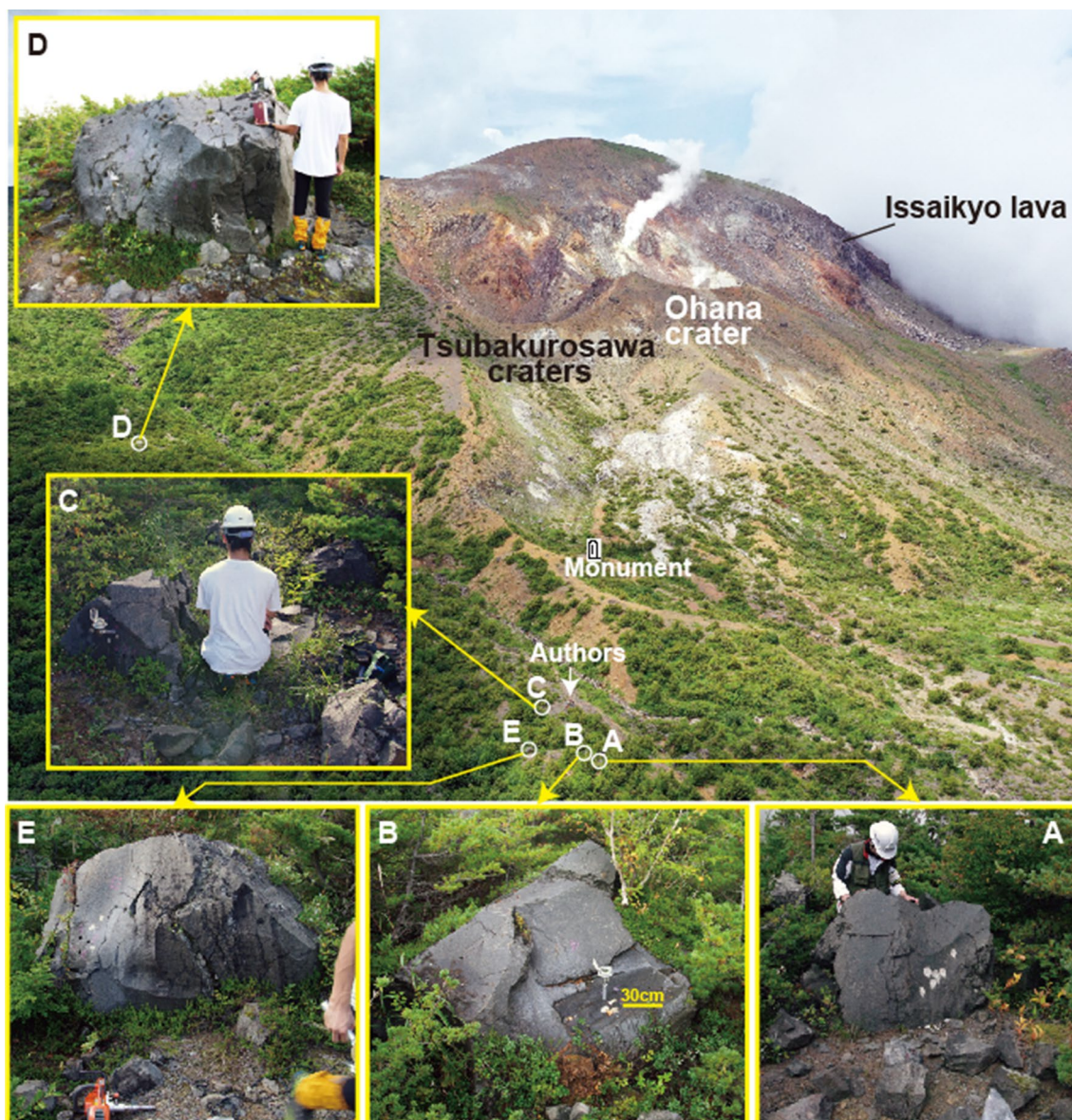


Fig. 2 Aerial photo of Tsubakurosawa craters from southeast (after Hasegawa et al. 2023). Five bombs for oriented sampling (A–E) are marked by circles. Note the authors near bombs C for scale. Monument: monument for Mr. Miura and Mr. Nishiyama. Insets shows close-up of the volcanic bombs. Note that these bombs are embedded in the ground with their interior parts partly exposed due to disintegration of the breadcrust surface

observed several times at the Ohana crater, such as in 1914, 1950 and 1977 CE. In the current study, we sampled volcanic bombs distributed mainly around the south of the Ohana and Tsubakurosawa craters. Based on ^{14}C ages of organic materials in the underlying phreatic eruption deposit, Yamamoto (2005) suggested that one of the bombs is from the Kamakura period (1331 CE) eruption. However, there has been no direct dating data for the volcanic bombs and the exact age remains unclear.

Sampling and analytical methods

Sampling and petrological analysis

Huge and glassy-breadcrust bombs containing large olivine phenocrysts are characteristically recognized at the surface south of Ohana and Tsubakurosawa craters of Azuma–Jododaira volcano (Fig. 2). For paleomagnetic studies, we carefully selected and sampled five bombs (A, B, C, D and E), avoiding steep slopes, or any evidence of secondary movement after their emplacement. All the bombs were more than 1 m in diameter and embedded in

the ground (Fig. 2). The breadcrust parts of all the bombs except D fell apart exposing the interior portion (Fig. 2). Six oriented cores (2.54 cm in diameter) were collected from the massive (non-cracked) interior portions of each bomb (Additional file 2: Table S1). The bombs are olivine pyroxene andesite, with slight variation of whole rock compositions ($\text{SiO}_2=58.35\sim 60.04$ wt.%, $\text{FeO}^*/\text{MgO}=1.55\sim 1.89$ wt.%, and $\text{K}_2\text{O}=1.48\sim 1.97$ wt.%) (Additional file 2: Table S2). In this study, the whole-rock chemistry was analyzed by X-ray fluorescence (XRF: RIGAKU PRIMUS II system, Ibaraki University) and the samples were prepared using the glass beads method of 1:2 dilution described by Hasegawa et al. (2019).

Magnetic analyses

Magnetic analyses carried out at Ibaraki University Japan, included measurement of the anisotropy of magnetic susceptibility (AMS) and natural remanent magnetization (NRM) prior to and following progressive thermal (THD) or alternating field (AFD) demagnetizations. AMS measurements were conducted using an AGICO Kappabridge KLY-3, with the aim of constraining the magnetic fabric of each bomb. Most samples were subsequently subjected to stepwise THD using a TD-48, ASC Scientific furnace up to a peak temperature of 630 °C. Alternating field demagnetization was conducted on samples from one volcanic bomb (bomb “D”) using an AGICO LDA-5 AF demagnetizer to a peak alternating field of 100 mT for checking coercivity and magnetic carrier minerals and consistency with the results of THD. Remanences were measured by an AGICO JR-6A. Characteristic remanent magnetization directions (ChRM) were calculated using principal component analysis (PCA) (Kirschvink 1980). Datapoints for ChRM calculation were selected from the most stable component trending towards the origin of the vector component plot. As a result, the maximum angular deviations (MAD) for THD samples (without bomb D) were less than 2.1° (Additional file 2: Table S1). The MAD values for bomb D were relatively larger, especially for AFD samples, but less than 8.4° (Additional file 2: Table S1). Unit (site) mean directions and 95% confidence intervals (α_{95}) were calculated from individual specimen ChRM directions using Fisher statistics (Fisher 1953).

Thermomagnetic curves were measured on 3–6 chip samples of ~10–100 mg for each bomb except D using a magnetic balance in Kochi University (NMB-89, Natsuhara Giken). For the measurement, induced magnetization was continuously monitored during a temperature cycle between room temperature and 700 °C under a field of 300 mT with vacuum condition (1–10 Pa). Hysteresis measurements were also conducted on 3–6 sister chip samples of ~10–100 mg for each bomb except D by

a vibrating sample magnetometer (MicroMag 3900 VSM, Lake Shore Cryotronics Inc., USA). A so-called Day plot (Day et al. 1977) was drawn based on the resultant key hysteresis parameters, namely, saturation magnetization (M_s), saturation remanent magnetization (M_{rs}), coercive force (B_c), and coercivity of remanence (B_{rc}). To characterize magnetic domain state in more detail, a chip sample of the bomb A was subjected to a measurement to construct a first-order reversal curve (FORC) diagram (Pike et al. 1999; Roberts et al. 2000, 2014) to map the distributions of coercivity (H_c) and magnetostatic interaction (H_u) at room temperature using the vibrating sample magnetometer. Calculation and analysis of the FORC diagram were performed using the FORCinel software version 3.08 released in 2022 (Harrison and Feinberg 2008).

Results and interpretations

Anisotropy of magnetic susceptibility (AMS)

Anisotropy of magnetic susceptibility data are summarized in Additional file 2: Table S1 and Fig. 3. T-Pj plots show a relatively low degree of anisotropy ($P_j < 1.051$), and a weak trend towards more oblate shapes with increasing Pj value. Each K_{\min} , K_{int} and K_{\max} is well-grouped within a single bomb (Fig. 3). The K_{\min} axes of bomb “B” are almost vertically oriented. However, the mean directions of K_{\min} and the lineation (clustering of K_{\max} orientations) for five bombs, including B, are randomly distributed.

Rock magnetic experiments

The thermomagnetic curves all show a single Curie temperature (T_c) mainly of ~260 to 320 °C and only minor differences are observed between the heating and cooling curves (Fig. 4). These suggest that the main magnetic carriers are titanomagnetites (TMs) with moderate Ti content that have not suffered from low-temperature oxidation (weathering). Of these, bombs A and B show a slightly lower T_c of ~260 °C (Fig. 4a, b) compared to the T_c of ~320 °C for bomb C (Fig. 4c), while bomb E exhibits intermediate characteristics between them (Fig. 4d). These behaviors seem consistent with the fact that bombs A and B were taken from adjacent and nearly identical locations, bomb C from a short distance away, and the bomb E from a point midway between these locations (Fig. 2).

The hysteresis data are distributed slightly to the right of the theoretical mixing curve for single-domain (SD) and multi-domain (MD) magnetite particles (Dunlop 2002) in the Day plot, with the volume fraction of MD being greater than ~90% in most cases (Additional file 1: Fig. S1a). Because the theoretical curve for Ti-rich TM moves towards the upper-right-hand region of the Day plot (Dunlop 2002), the distribution is consistent with

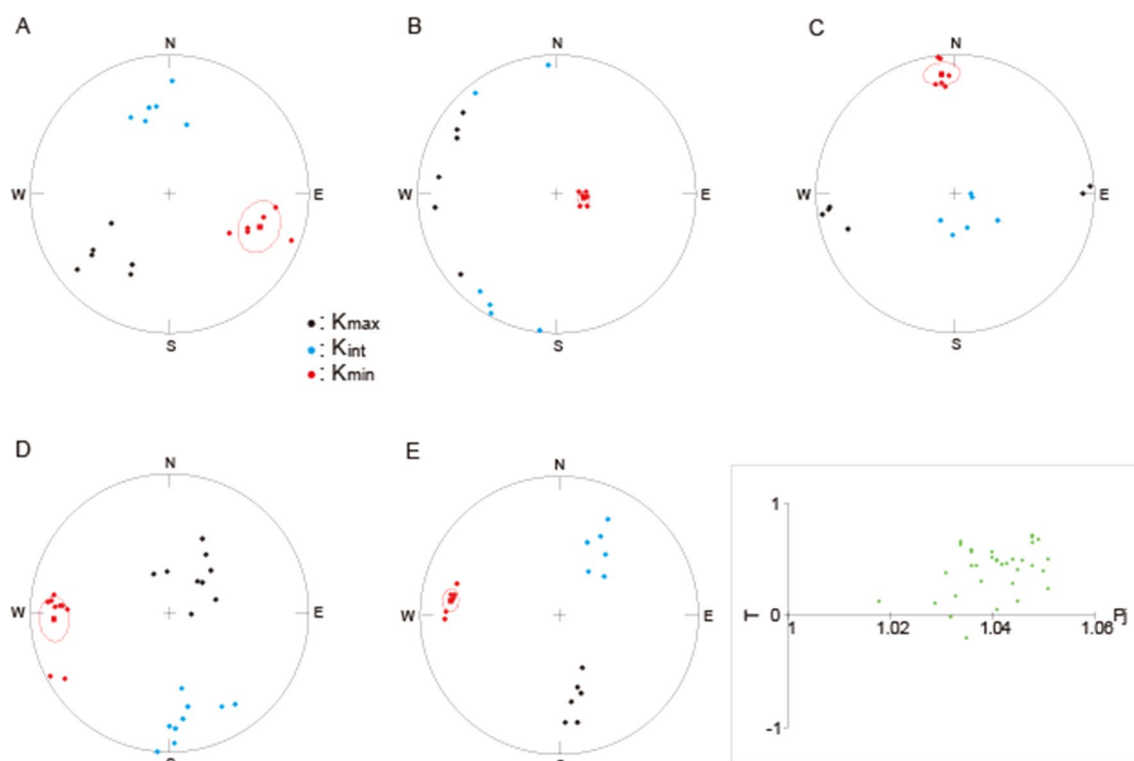


Fig. 3 Lower-hemisphere stereographic projections of the principal axes of magnetic susceptibility (AMS) for each unit. Black: K_{\max} , blue: K_{int} , red: K_{\min} . Red square represents site mean direction of K_{\min} axes with the 95% confidence ellipses. Bottom right box shows the plot of anisotropy degree (P_j) versus shape parameter (T) for all data

the dominant presence of TMs with T_c of ~ 260 to 320 °C as the main magnetic carrier. A large contribution of MD-like remanence carriers is confirmed from the FORC diagram (Additional file 1: Fig. S1b), as open MD-like contours are clearly recognized for the ranges of B_c from 0 to ~ 20 mT and B_u from ~ -50 to ~ 50 mT. This is consistent with the AFD result that a large reduction in NRM is observed by ~ 20 mT (see next section: Fig. 5f). However, a central ridge along the B_c axis of the FORC diagram, extending to ~ 60 mT at $B_u \sim 0$ is also recognizable, which is the indication of the presence of some noninteracting SD-like magnetic particles. In the AFD result, the characteristic remanence component is extracted from the coercivity interval between 20 and 60 mT (Additional file 2: Table S1), and this is considered to be carried by SD-like magnetic particles.

Demagnetization behavior and remanent magnetization directions

From THD experiments, all the samples show a single stable component of magnetization that decreases linearly towards the origin of the vector component plot, after removal of the secondary viscous component. In most cases, the ChRM directions can be resolved from

the temperature intervals above 100–200 °C and main reduction in the natural remanent magnetization (NRM) are observed below ~ 260 – 320 °C which are the estimated Curie temperature of main phase (Additional file 2: Table S1; Fig. 5a–e). During AFD, samples lost ca. 90% of their remanence intensity at applied peak fields lower than 45 mT (Additional file 2: Table S1; Fig. 5f). These data support the result of rock magnetic experiments that the main carrier magnetic mineral is titanomagnetite (TM) with relatively low coercivity. The ChRM directions of the AFD experiment (on 3 samples from bomb D) are almost consistent with those of THD. We then combined the ChRM directions of both AFD and THD to calculate the site mean of remanent magnetization direction for bomb D. The ChRM directions for specimens from all 5 bombs (A, B, C, D and E) are well-grouped with α_{95} values 2.5° or less. The mean directions for the bombs show good agreement with the range in declination from 351.9 to 356.8°, and in inclination from 48.8 to 51.4° and are not different with the 95% confidence limit from each other (Table 1; Fig. 6). Based on these data, it is suggested that all the five volcanic bombs landed at or above unblocking temperature (~ 200 to 480 °C) and were not moved nor re-heated after the emplacement. The overall

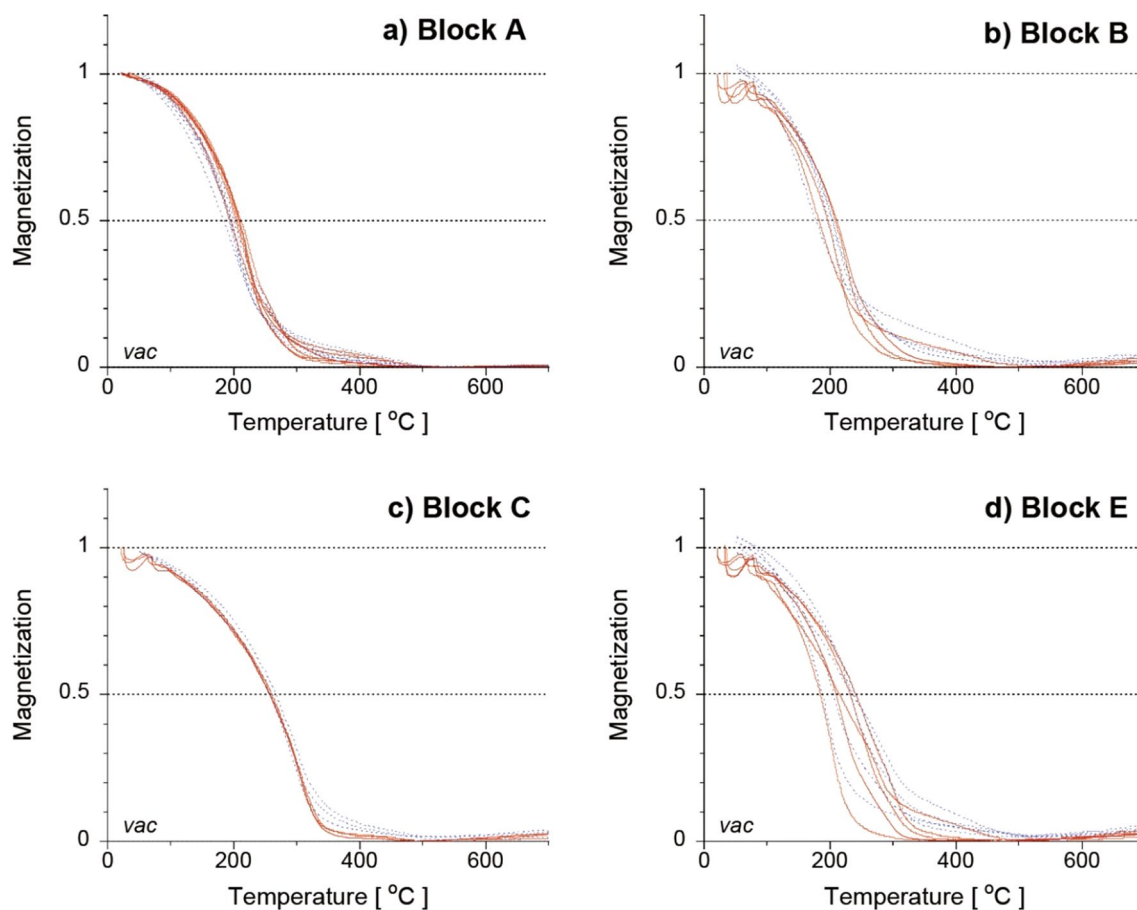


Fig. 4 Thermomagnetic curves of the chip samples from bombs A (a), B (b), C (c), and E (d). Red (blue dashed) lines indicate heating (cooling) cycle

mean paleomagnetic direction (all-site mean direction an average over the 5 means for each bomb: total number of specimens $N=33$) is $\text{Dec}=355.5^\circ$, $\text{Inc}=49.8^\circ$ with a 95% confidence of 1.6° , updated from the values of Hasegawa et al. (2023).

Discussion

Paleomagnetic dating

The ChRM directions of samples from the five volcanic bombs show an overall good agreement as evidenced by overlap of their mean directions at the 95% confidence level (Fig. 6; Table 1). The overall mean direction (updated by adding the result of AFC experiment from Hasegawa et al. 2023) is defined as $\text{Dec}=355.5^\circ$, $\text{Inc}=49.8^\circ$ with 95% confidence of 1.6° . Although the five bombs have slight variations both in rock magnetic properties and chemical compositions, they provide very consistent paleomagnetic directions, as would be expected if they record the geomagnetic field when the bombs were emplaced and cooled. Hasegawa et al. (2023) suggested that the five bombs are from Meiji period eruption based on the correlation between the mean ChRM

direction and the available paleosecular variation (PSV) curve. Here, we quantitatively verify the result based on the updated mean direction and reasonable field models with mathematic computation tool.

Based on the global historical geomagnetic field model “*gufm1*” (Jackson et al. 2000), the magnetic field direction at the Azuma–Jododaira volcano (Lat.= 140.25°E , Long.= 37.72°N , Alt.=1581 m) in 5th June 1893 CE is $\text{Dec}=355.13^\circ$ and $\text{Inc}=51.36^\circ$. The *gufm1* is a time-dependent field model from an extensive compilation of historical records, observatory annual means, and satellite observations of the magnetic field during 1590–1990 CE (Jackson et al. 2000). Our overall mean direction well matches the model field direction by *gufm1* within the 95% confidence interval. Next, we conducted paleomagnetic dating by comparing the overall mean direction to the locally constructed paleosecular variation (PSV) curve for Japan, as the JRFM2K.1 (Hatakeyama 2013). The JRFM2K.1 is compiled from several thousands of archaeomagnetic data mainly obtained from buried kilns and baked earths, reconstructing the geomagnetic secular variation model for the past 2000 years

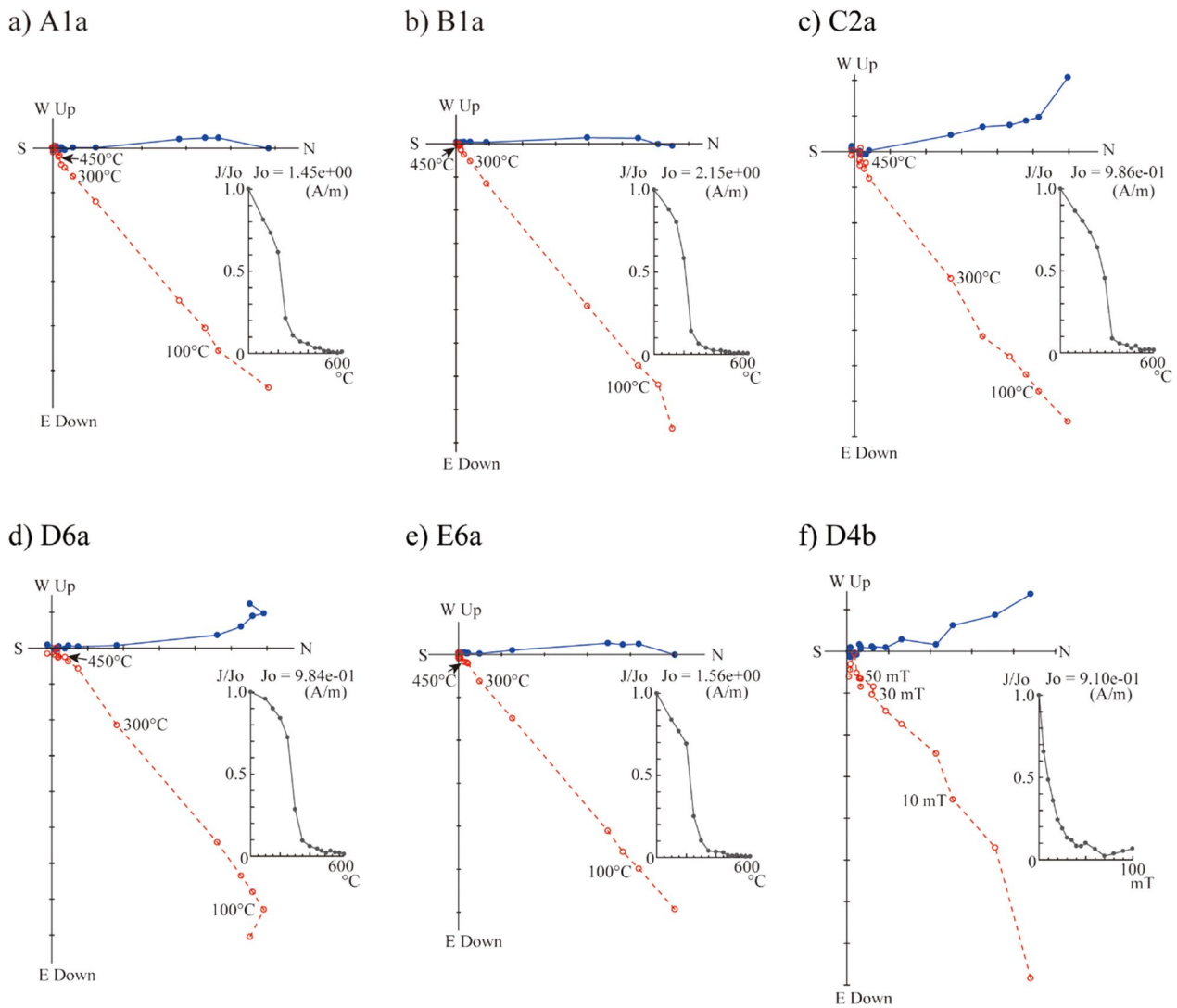


Fig. 5 Orthogonal vector end-point plots for thermal demagnetization results of NRM for representative specimens from each site. Solid blue and open red symbols are projections onto horizontal and vertical planes, respectively. D4b was subjected to alternating field demagnetization (AFD)

Table 1 Site mean ChRM direction for each volcanic bomb (A–E) together with their overall (all-site) mean direction at the south of Tsubakurosawa craters

Bomb (site)	D_m (deg)	I_m (deg)	α_{95} (deg)	k	N	Coordination
A	356.1	50.1	1.0	4367.0	6	37°43'16.4"N, 140°14'57.8"E
B	356.0	49.4	1.5	1962.7	6	37°43'16.5"N, 140°14'57.6"E
C	351.9	48.8	2.5	721.6	6	37°43'17.0"N, 140°14'56.7"E
D	356.8	51.4	2.5	438.1	9	37°43'19.7"N, 140°14'47.6"E
E	357.0	49.4	1.3	2558.7	6	37°43'16.4"N, 140°14'56.9"E
All-site mean	355.5	49.8	1.6		5*	

D_m , I_m , α_{95} , k and N indicate mean declination, mean inclination, 95% confidence limit angle, precision parameter, number of specimens used to determine the site-mean, respectively. Data of other than site D are from Hasegawa et al. (2023). Those of D are updated from Hasegawa et al. (2023)

* The all-site mean direction an average over the 5 means for each bomb

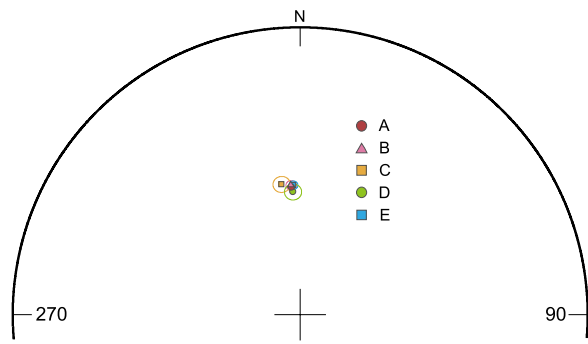


Fig. 6 Equal area projection of mean characteristic remanent magnetization (ChRM) directions for each volcanic bomb (A~E) collected at the south of Tsubakurosawa craters (after Hasegawa et al. 2023). Symbols (circle, triangle, and square in different color) indicate the individual mean directions, while ellipses denote their 95% confidence limit angles (α_{95})

in Japan (Hatakeyama 2013). We used the directional record from 400 to 2000 CE as the accuracy and precision of the PSV curve for 1 to 400 CE is particularly low due to the sparse data for this time period. Our overall mean direction was matched to the JRFM2K.1 model using the MATLAB-based dating tool of Pavón-Carrasco et al. (2011) after relocation to 140.25°E and 37.72°N (Azuma–Jododaira volcano). The combination of probability density functions of declination and inclination (95% confidence) yields two matching age ranges estimated: 400–498 CE, and 1829–1900 CE (Fig. 7). The younger matched age range encompasses the 1893–1895 CE of Meiji eruption. The older matched age range (400–498 CE) shows stronger peak comparing to younger one. However, recent geological studies (Yamamoto 2005, Furukawa et al. 2018; Imura et al. 2021; Hasegawa et al. 2023) reported no eruption deposits around 400–500 CE. In addition, Yamamoto (2005) obtained many ^{14}C ages of around 1300 CE from organic materials in the phreatic eruption deposit that underlies the volcanic bombs

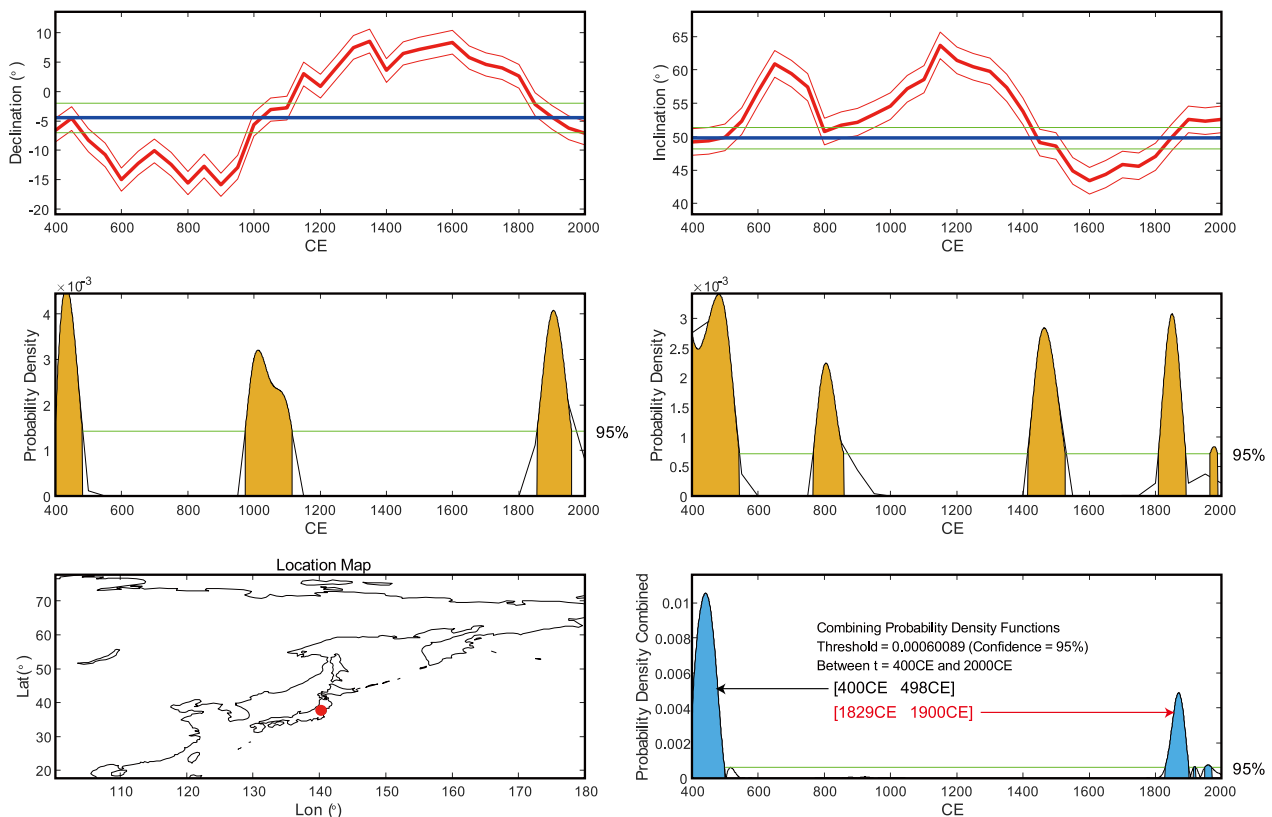


Fig. 7 Result of paleomagnetic dating using MATLAB archaeomagnetic dating tool (Pavón-Carrasco et al. 2011), based on the paleosecular variation (PSV) curve reference model (JRFM2K.1 by Hatakeyama 2013). PSV curve for the declination, inclination (every 50 years) are shown as thick red lines (thin red lines for the associated α_{95} % level estimated as 2° for convenience), together with the probability density curves (in orange-shade below each PSV curve). Paleomagnetic declination, inclinations of our samples (relocated to Azuma–Jododaira as 140.25E and 37.72N) are shown in the PSV curve graphs as blue straight lines; the green dashed lines above and below are the associated α_{95} % levels. The final combined probability density curves are shown in light blue-shade (the 95% confidence levels are shown as a green line). Preferred palaeomagnetic age estimates (1829–1900 CE) is arrowed and shown by red color

in this area. Moreover, the volcanic bombs we sampled were situated on the current surface and not covered by any young ash. Consequently, it is concluded that the olivine-rich and large, breadcrust bombs at the south of Tsubakurosawa craters were formed during the Meiji period (1893–1895 CE) eruption. Based on the ^{14}C ages of underlying phreatic eruption deposits as mentioned above, Yamamoto (2005) suggested that the huge (4 m in diameter) bombs in this area are from the Kamakura period (1331 CE) eruption. However, it should be noted that the ^{14}C ages are not directly from the bomb samples. More detailed geological description, deciphering historical documents, and discussions are reported in Hasegawa et al. (2023).

Eruption style inferred from the emplacement condition of volcanic bombs

Vulcanian eruptions are interpreted as rupturing of a cap rock (plug) from the uppermost part of a volcanic conduit (Wright et al. 2006). Vulcanian eruption products are generated as a result of explosion and fragmentation of the lava plug in the conduit system. Breadcrust bombs with andesitic chemical composition are some of the typical products of vulcanian eruptions (Wright et al. 2006), suggesting that the bombs we analyzed are the products of vulcanian activity. In this section, we discuss the processes and style of the Meiji period eruption on the basis of the paleomagnetic data that was not presented in Hasegawa et al. (2023).

Anisotropy of magnetic susceptibility (AMS) fabrics are often used for investigating the flow directions of continuous magmatic fluid, such as lava flow. The $K_{\text{max}}-K_{\text{int}}$ plane is generally parallel to the flow-related fabrics of a fluidal lava flow or dike intrusion (Kapawar et al. 2021). The AMS plots showing vertically clustered K_{min} and horizontally distributed K_{max} and K_{int} , like that of bomb B in this study (Fig. 3), are typically observed in cases of fluidal lava flows (Herrero-Bervera et al. 2002; Zhu et al. 2003; Nagaraju and Parashuramulu 2019; Kapawar et al. 2021). In this case, the direction of K_{max} tends to represent the flow alignment of lava (and dike). It was difficult to identify flow textures in the volcanic bombs in the field due to the massive and glassy lithology. However, the random distribution of K_{min} (perpendicular to the $K_{\text{max}}-K_{\text{int}}$ plane) of the five bombs (Fig. 3) suggests that each bomb was derived from a solidified plug of lava in the conduit, and it was fragmented and ejected in pieces by vulcanian explosions (e.g., Iguchi et al. 2008). The AMS fabric of the lava plug was frozen-in below the solidification point, which is generally 800–1000 °C at 1 atm for andesitic to basaltic magma

(Lambert and Wyllie 1974; Stern et al. 1975). After that, each fragmented piece of the bomb was rotated during the flight and landed at the surface, resulting in random K_{min} orientations. However, they were still hot at the landing, and it is considered that the ChRM direction of each bomb was blocked during cooling from above their Curie temperature of ~260 to 320 °C to ambient temperature, after the emplacement. The AMS feature of bomb B showing almost vertical K_{min} axes would not be from gravitational compaction and deformation at (or after) the landing but just a coincidence, because the anisotropy degree P_j of bomb B is not so large and not different from that of other bombs ($P_j=1.029-1.051$) (Additional file 2: Table S1).

Concluding remarks

Hasegawa et al. (2023) already estimated the eruption age of the volcanic bombs around the Tsunakurosawa craters based on paleomagnetic dating by the THD experiment. However, this paper further improves the technique and results by combining data from the thermomagnetic analysis, hysteresis measurements, AMS and AFD experiments, XRF chemical analysis, and MATLAB-based archaeomagnetic dating. The results of this paper validate the utility of volcanic bombs for further paleomagnetic research. It can be a powerful paleomagnetic tool if we can access the area around the source craters and safely perform oriented sampling of the volcanic bombs. The effective sampling technique of volcanic bombs for paleomagnetic dating can be summarized as follows. At first, collection of multiple samples from at least four to five (A to E in this study) bombs is essential to obtain reliable paleomagnetic data. It should be checked if the petrological features, such as petrography, mineral assemblage, and chemical composition, are common for these samples (bombs). Furthermore, the sampling sites and conditions of each bomb should be carefully selected to avoid the possibility of secondary movement (tilting and rotation). Large bombs embedded in the ground have very low possibility of the secondary tilting and rotation. Samples from the interior parts of large volcanic bombs would be ideal, because they are likely to have cooled more slowly and had a greater chance to acquire stable thermal magnetization at higher temperatures. The AMS measurement is also helpful in evaluating the temperature conditions at the time of ejection, which is decisive for eruption style. Finally, a well-established paleo secular variation curve and a combination with geological data and ^{14}C age are required for high-resolution constraints on the paleomagnetic dating method.

Supplementary Information

The online version contains supplementary material available at <https://doi.org/10.1186/s40623-023-01931-3>.

Additional file 1: Figure S1. (a) Day plot for the hysteresis data from chip samples of bombs A, B, C, and E. Threshold values for single domain (SD) and multi-domain (MD) fields, and a theoretical SD–MD mixing curve for magnetite are also indicated by solid lines and a dotted curve, respectively, according to Dunlop (2002). (b) FORC diagram drawn from the measurement result for a chip sample of bomb A.

Additional file 2: Table S1. Paleomagnetic data for each sample (core). Sample “A1a” is from more interior part than “A1b”. **Table S2.** Whole-rock major element compositions and phenocryst assemblages of samples from volcanic bombs A to E. ol: olivine, cpx: clinopyroxene, opx: orthopyroxene, pl: plagioclase, ox: Fe–Ti oxides. FeO*: total iron calculated to be FeO.

Acknowledgements

We appreciate Kazuma Suzuki and Atsuharu Tomaru for helping in oriented sampling of volcanic bombs around Tsubakurosawa craters. We are also grateful to the Fukushima Local Meteorological Observatory, the Fukushima Prefecture Governments, the Fukushima Office of Ministry of the Environment, and Ministry of Agriculture, Forestry and Fisheries for granting permission to enter and collect samples in the protected areas. We thank Dr. Festus Aka for reading our manuscript. We wish to express our gratitude to the Editor, Gillian Turner, and two reviewers, Geoffrey Lerner and anonymous reviewer.

Author contributions

TH and YY wrote the manuscript. TH, BK, SS, TI, MB, KT, and TO participated in the field survey and sampling. TH, SS, CK, MO, and YY performed magnetic experiments and measurements. SS, TI, and MB carried out petrological analyses. All authors participated in the interpretation and discussion of the results. All authors read and approved the final manuscript.

Funding

This research was supported by Japan and JSPS KAKENHI Grant Number JP21H01166, JP22K18726 (TH), JP21H01171 (YY) and the Integrated Program for Next Generation Volcano Research and Human Resource Development funded by MEXT.

Availability of data and materials

The data sets used and/or analyzed during the current study are available from the corresponding author on reasonable request.

Declarations

Competing interests

The authors declare that the research was conducted in the absence of any commercial or financial relationships that could be construed as a potential competing interest.

Author details

¹Department of Earth Sciences, Ibaraki University, 2-1-1, Bunkyo, Mito 310-8512, Japan. ²National Research Institute for Earth Science and Disaster Resilience, 3-1 Tennodai, Tsukuba-Shi, Ibaraki 305-0006, Japan. ³Marine Core Research Institute, Kochi University, Monobe B200, Nankoku, Kochi 783-8502, Japan. ⁴Faculty of Science, Yamagata University, 1-4-12, Kojirakawamachi, Yamagata 990-8560, Japan. ⁵Graduate School of International Resource Sciences, Akita University, Tegatagakuenmachi 1, Akita, Akita 010-0852, Japan.

Received: 8 July 2023 Accepted: 5 November 2023

Published: 16 November 2023

References

Arrighi S, Tanguy J-C, Rosi M (2006) Eruptions of the last 2200 years at Vulcano and Vulcanello (Aeolian Islands, Italy) dated by high-accuracy

- archaeomagnetism. *Phys Earth Planet Inter* 159:225–233. <https://doi.org/10.1016/j.pepi.2006.07.010>
- Böhnel H, Pavón-Carrasco FJ, Sieron K, Mahgoub AN (2016) Palaeomagnetic dating of two recent lava flows from Ceboruco volcano, western Mexico. *Geophys J Int* 207:1203–1215. <https://doi.org/10.1093/gji/ggw310>
- Cañón-Tapia E (2017) Mechanism of formation of volcanic bombs: insights from a pilot study of anisotropy of magnetic susceptibility and preliminary assessment of analytical models. *Bull Volcanol* 79:49. <https://doi.org/10.1007/s00445-017-1136-6>
- Cole RP, Ohneiser C, White JDL, Townsend DB, Leonard GS (2019) Paleomagnetic evidence for cold emplacement of eruption-fed density current deposits beneath an ancient summit glacier, Tongariro volcano, New Zealand. *Earth Planet Sci Lett* 522:155–165. <https://doi.org/10.1016/j.epsl.2019.07.004>
- Day R, Fuller M, Schmidt VA (1977) Hysteresis properties of titanomagnetites: grain size and compositional dependence. *Phys Earth Planet Inter* 13:260–267. [https://doi.org/10.1016/0031-9201\(77\)90108-X](https://doi.org/10.1016/0031-9201(77)90108-X)
- Dunlop DJ (2002) Theory and application of the Day plot (Mrs/Ms versus Hcr/Hc) 1. Theoretical curves and tests using titanomagnetite data. *J Geophys Res* 107:2056. <https://doi.org/10.1029/2001JB000486>
- Fisher RA (1953) Dispersion on a sphere. *Proc R Soc London* 217:295–305. <https://doi.org/10.1098/rspa.1953.0064>
- Furukawa R, Nakano S, Takahashi Y, Yamamoto T (2018) Geology of the Azuma Yama District, with Geological Sheet Map at 1:50,000, Geological Survey of Japan, pp77 (in Japanese with English abstract).
- Greve A, Turner GM (2017) New and revised palaeomagnetic secular variation records from post-glacial volcanic materials in New Zealand. *Phys Earth Planet Inter* 269:1–17. <https://doi.org/10.1016/j.pepi.2017.05.009>
- Harrison RJ, Feinberg JM (2008) FORCinel: an improved algorithm for calculating first-order reversal curve distributions using locally weighted regression smoothing. *Geochem Geophys Geosyst* 9:Q05016. <https://doi.org/10.1029/2008GC001987>
- Hasegawa T, Aka FT, Miyabuchi Y, Nche LA, Kobayashi T, Kaneko K, Nkengmatia A, Asaah E, Kankeu B, Issa Ohba T, Kusakabe M, Hell JV (2019) Eruption history and petrogenesis of rocks from Nyos volcano (NW Cameroon): evidence from lithostratigraphy and geochemistry. *J Volcanol Geotherm Res* 378:52–71. <https://doi.org/10.1016/j.jvolgeores.2019.04.003>
- Hasegawa T, Kikuchi B, Shibata S, Imura T, Ban M, Tsunematsu K, Yamamoto Y, Ohba T, Suzuki K, Tomaru A, Kusu C, Okada M (2023) Magma had ejected in CE 1893 eruption (Meiji eruption) at Azuma-Jododaira volcano, Fukushima: Inferred from paleomagnetic dating for large volcanic bombs around Tsubakurosawa craters. *Bull Volcanol Soc Jpn* 68:189–196 (in Japanese with English abstract). https://doi.org/10.18940/kazan.68.3_189
- Hatakeyama T (2013) Online database of archaeomagnetism in Japan. American Geophysical Union, Fall Meeting 2013, abstract id. GP41B-1123. <http://mag.ifst.ous.ac.jp/en>
- Herrero-Bervera E, Cañón-Tapia E, Walker GPL, Tanaka H (2002) Magnetic fabric study and inferred flow directions of lavas of the old Pali Road, O’ahu, Hawaii. *J Volcanol Geotherm Res* 118:161–171. [https://doi.org/10.1016/S0377-0273\(02\)00255-X](https://doi.org/10.1016/S0377-0273(02)00255-X)
- Iguchi M, Yakiwara H, Tameguri T, Hendrasto M, Hirabayashi J (2008) Mechanism of explosive eruption revealed by geophysical observations at the Sakurajima, Suwanosejima and Semeru volcanoes. *J Volcanol Geotherm Res* 178:1–9. <https://doi.org/10.1016/j.jvolgeores.2007.10.010>
- Imura T, Ohba T, Horikoshi K (2021) Geologic and petrologic evolution of subvolcanic hydrothermal system: a case on pyroclastic deposits since the 1331 CE eruption at Azuma-Jododaira volcano, central Fukushima, North-Eastern Japan *J Volcanol Geotherm Res* 416:107274. <https://doi.org/10.1016/j.jvolgeores.2021.107274>
- Jackson A, Jonkers ART, Walker M (2000) Four centuries of geomagnetic secular variation from historical records. *Philos Trans R Soc London Ser A* 358:957–990. <https://doi.org/10.1098/rsta.2000.0569>
- Kapawar MR, Mamilla V, Sangode SJ (2021) Anisotropy of magnetic susceptibility study to locate the feeder zone and lava flow directions of the Rajmahal Traps (India): implications to Kerguelen mantle plume interaction with Indian Plate. *Phys Earth Planet Inter* 313:106692. <https://doi.org/10.1016/j.pepi.2021.106692>
- Kirschvink JL (1980) The least-squares line and plane and the analysis of paleomagnetic data. *Geophys J Int* 62:699–718. <https://doi.org/10.1111/j.1365-246X.1980.tb02601.x>

- Kojo Y, Kalin R, Long A (1994) High precision wiggle matching in radiocarbon dating. *J Archaeol Sci* 21:475–479. <https://doi.org/10.1006/jasc.1994.1047>
- Kósić S, Hasegawa T, Danišić M, Németh K, Okada M, Friedrichs B, Schmitt AK (2023) Multi-method constraints on the age and timescale of silicic small-volume eruptions of Puketerata Volcanic Complex, Taupō Volcanic Zone, New Zealand. *Earth Planets Space* 75:107. <https://doi.org/10.1186/s40623-023-01861-0>
- Lambert IB, Wyllie PJ (1974) Melting of tonalite and crystallization of andesite liquid with excess water to 30 kilobars. *J Geol* 82:88–97. <https://doi.org/10.1086/627938>
- Matsumoto A, Nakano S, Furukawa R, Yamamoto T (2018) History of Azuma Volcano based on K – Ar age determinations. *Bull Geol Surv Jpn* 69:153–163 (in Japanese with English abstract). <https://doi.org/10.9795/bullgsj.69.153>
- Nagaraju E, Parashuramulu V (2019) AMS studies on a 450 km long 2216 Ma dyke from Dharwar craton, India: implications to magma flow. *Geosci Front* 10:1931–1939. <https://doi.org/10.1016/j.gsf.2018.12.003>
- Omori F (1893) Summary of field survey about explosion from Azuma Volcano, Publications of the Earthquake Investigation Committee. 1: 60–62 (in Japanese).
- Pavón-Carrasco FJ, Rodríguez-González J, Osete ML, Torta JM (2011) A Matlab tool for archaeomagnetic dating. *J Archaeol Sci* 38:408–419. <https://doi.org/10.1016/j.jas.2010.09.021>
- Pike CR, Roberts AP, Verosub KL (1999) Characterizing interactions in fine magnetic particle systems using first order reversal curves. *J Appl Phys* 85:6660–6667. <https://doi.org/10.1063/1.370176>
- Pivarunas AF, Blatter DL, Muffler LJP, Clynne MA, Calvert AT, Harrison LN, Christiansen RL (2022) Paleomagnetically defined brief lifespans for two large shield volcanoes in the Cascades Arc. *J Volcanol Geotherm Res* 434:107740. <https://doi.org/10.1016/j.jvolgeores.2022.107740>
- Roberts AP, Pike CR, Verosub KL (2000) First-order reversal curve diagrams: a new tool for characterizing the magnetic properties of natural samples. *J Geophys Res Solid Earth* 105(B12):28461–28475. <https://doi.org/10.1029/2000JB900326>
- Roberts AP, Heslop D, Zhao X, Pike CR (2014) Understanding fine magnetic particle systems through use of first-order reversal curve diagrams. *Rev Geo-Phys* 52:557–602. <https://doi.org/10.1002/2014RG000462>
- Roperch P, Chauvin A, Lara LE, Moreno H (2015) Secular variation of the Earth's magnetic field and application to paleomagnetic dating of historical lava flows in Chile. *Phys Earth Planet Inter* 242:65–78. <https://doi.org/10.1016/j.pepi.2015.03.005>
- Speranza F, Pompilio M, D'Ajello Caracciolo F, Sagnotti L (2008) Holocene eruptive history of the Stromboli volcano: constraints from paleomagnetic dating. *J Geophys Res* 113:BD9101. <https://doi.org/10.1029/2007JB005139>
- Stern CR, Huang WL, Wyllie PJ (1975) Basalt-Andesite-Rhyolite-H₂O: crystallization intervals with excess H₂O and H₂O-undersaturated liquidus surfaces to 35 kolbras, with implications for magma genesis. *Earth Planet Sci Lett* 28:189–196. [https://doi.org/10.1016/0012-821X\(75\)90226-5](https://doi.org/10.1016/0012-821X(75)90226-5)
- Tanguy JC, Le Goff M, Principe C, Arrighi S, Chillemi V, Paiotti A, La Delfa S, Patane G (2003) Archeomagnetic dating of Mediterranean volcanics of the last 2100 years: validity and limits. *Earth Planet Sci Lett* 211:111–124. [https://doi.org/10.1016/S0012-821X\(03\)00186-9](https://doi.org/10.1016/S0012-821X(03)00186-9)
- Turner GM, Corkill RM (2023) NZPSV1k.2023 and NZPSV11k.2023: holocene palaeomagnetic secular variation master records for New Zealand. *Phys Earth Planet Inter* 344:107093. <https://doi.org/10.1016/j.pepi.2023.107093>
- Wright HMN, Cashman KV, Rosi M, Cioni R (2006) Breadcrust bombs as indicators of Vulcanian eruption dynamics at Guagua Pichincha volcano. *Ecuador Bull Volcanol* 69:281–300. <https://doi.org/10.1007/s00445-006-0073-6>
- Yamamoto T (2005) Eruptive history of Azuma volcano, NE Japan, during last 7,000 years: stratigraphy and magma-plumbing system of the Azuma-Jododaira products. *J Geol Soc Jpn* 111:94–111. <https://doi.org/10.5575/geosoc.111.94>
- Yokoyama M (1893) Explosion of Azuma Volcano. *J Geogr (chigaku Zasshi)* 5:533–541. <https://doi.org/10.5026/jgeography.5.533>
- Zhu R, Shi C, Liu Q (2003) Anisotropy of magnetic susceptibility of Hannuoba basalt, northern China: constraints on the vent position of the lava sequences. *Geophys Res Lett* 30:1066. <https://doi.org/10.1029/2002GL016215>

Publisher's Note

Springer Nature remains neutral with regard to jurisdictional claims in published maps and institutional affiliations.

Submit your manuscript to a SpringerOpen® journal and benefit from:

- Convenient online submission
- Rigorous peer review
- Open access: articles freely available online
- High visibility within the field
- Retaining the copyright to your article

Submit your next manuscript at ► [springeropen.com](https://www.springeropen.com)